

Discovering Interpretable Directions in the Semantic Latent Space of Diffusion Models

René Haas
IT University of Copenhagen
renha@itu.dk

Inbar Huberman-Spiegelglas*, Rotem Mulayoff*, Tomer Michaeli
Technion – Israel Institute of Technology
{inbarhub, rotem.mulayof}@gmail.com, tomer.m@ee.technion.ac.il

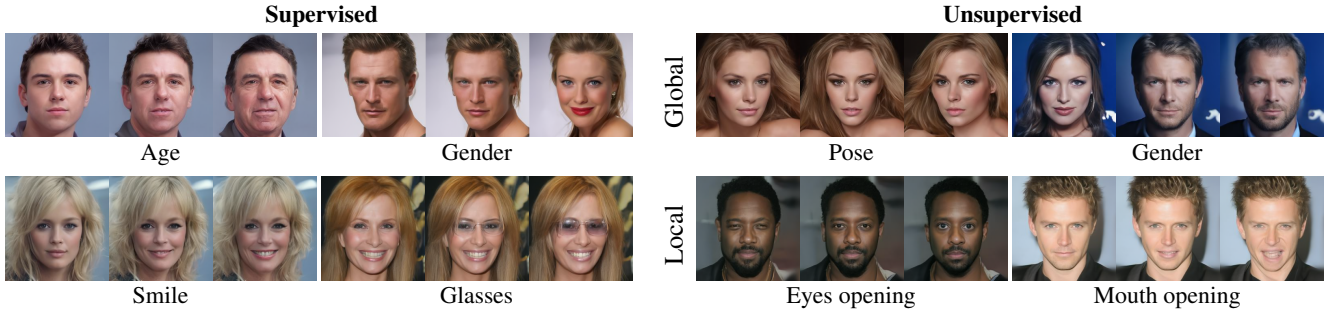


Figure 1: **Our semantic image editing.** We present new methods for finding interpretable disentangled semantic directions in the latent space of DDMs. Specifically, we propose a supervised (left) and two unsupervised (right) methods, where the latter finds either global directions based on a collection of images or local directions based on the analysis of a single sample.

Abstract

Denoising Diffusion Models (DDMs) have emerged as a strong competitor to Generative Adversarial Networks (GANs). However, despite their widespread use in image synthesis and editing applications, their latent space is still not as well understood. Recently, a semantic latent space for DDMs, coined ‘h-space’, was shown to facilitate semantic image editing in a way reminiscent of GANs. The h-space is comprised of the bottleneck activations in the DDM’s denoiser across all timesteps of the diffusion process. In this paper, we explore the properties of h-space and propose several novel methods for finding meaningful semantic directions within it. We start by studying unsupervised methods for revealing interpretable semantic directions in pretrained DDMs. Specifically, we show that global latent directions emerge as the principal components in the latent space. Additionally, we provide a novel method for discovering image-specific semantic directions by spectral analysis of the Jacobian of the denoiser w.r.t. the latent code. Next, we extend the analysis by finding directions in a supervised fashion in unconditional DDMs. We demonstrate how such directions can be found by relying on either a labeled data set of real images or by annotating gener-

ated samples with a domain-specific attribute classifier. We further show how to semantically disentangle the found direction by simple linear projection. Our approaches are applicable without requiring any architectural modifications, text-based guidance, CLIP-based optimization, or model fine-tuning.

1. Introduction

Denoising Diffusion Models (DDMs) [36] have emerged as a strong alternative to Generative Adversarial Networks (GANs) [5]. Today, they outperform GANs in unconditional image synthesis [3], a task in which GANs have been dominating in recent years. Besides synthesizing high-quality and diverse images, unconditional DDMs are also being used for conditional synthesis tasks by guiding them on various user inputs [9], such as a user-provided reference image [13, 17] or a text-prompt by utilizing Contrastive Language-Image Pretraining (CLIP) [22]. Conditional DDMs have also seen great success, particularly in the context of text-based synthesis. Specifically, recent large-scale text-conditional systems like DALL-E [26, 25], Stable Diffusion [27] and Imagen [32] have sparked a surge of research related to text-driven image editing using DDMs [19, 18, 4, 30, 11, 12, 7, 40, 2]. However, despite their pop-

*These authors contributed equally to this work.

ularity, it is still not well understood how to leverage the latent space of DDMs for semantic image editing in the unconditional setting, *i.e.*, in the absence of CLIP-guidance and without conditioning on a reference image. While there has been extensive research on finding disentangled editing directions in the latent space of unconditional GANs [1, 33, 10, 6, 35, 38, 24], comparatively little work has been done on this topic for unconditional DDMs.

Recently, Kwon *et al.* [14] proposed a semantic latent space for DDMs, coined ‘*h*-space’. In this paper, we leverage the editing capabilities of *h*-space and explore several supervised and unsupervised methods for finding interpretable editing directions in unconditional DDMs.

We start by proposing two unsupervised methods. In Sec. 4 we demonstrate that interpretable editing directions, like pose, gender, and age emerge as the principal components in the semantic latent space. Additionally, we propose a novel unsupervised method for discovering image-specific semantic directions resulting in highly localized edits like opening/closing of the mouth and eyes that can be applied to other samples. We illustrate a selection of these unsupervised editing directions in Fig. 1 (right pane). To the extent of our knowledge, we are the first to show that semantically meaningful editing directions can be found in unconditional DDMs in a fully unsupervised fashion.

Next, in Sec. 5 we utilize the linear properties of the semantic latent space and propose a simple supervised method for finding interpretable editing directions, like age and gender or the appearance of glasses or a smile. We illustrate examples of these edits in Fig. 1 (left pane). We demonstrate our approach both by using a facial expression data set of real images and by annotating samples generated by the model with a pretrained attribute classifier. We further propose a simple method for disentangling directions that affect multiple attributes.

Our approaches allow for intuitive and semantically disentangled image editing and can be applied to the latent space of DDMs without requiring any CLIP guidance, fine-tuning, optimization, user-provided reference images or any adaptations to the architecture of existing DDMs.

2. Related work

2.1. The latent space of diffusion models

GANs have a well-defined latent space suitable for semantic editing. Whether DDMs possess such a convenient latent space is still a topic of ongoing research. Here we review two approaches for defining a latent space in DDMs.

In DDIM [37], the generative process is a deterministic mapping from a Gaussian noise vector $\mathbf{x}_T \sim \mathcal{N}(\mathbf{0}, \mathbf{I})$ to a sampled image \mathbf{x}_0 . Here, Song *et al.* [37] regard the noise \mathbf{x}_T as the latent representation. DDIM has the property that fixing \mathbf{x}_T leads to images with similar high-level

features irrespective of the length of the generative process. Furthermore, interpolating between two latent codes $\mathbf{x}_T^{(1)}$ and $\mathbf{x}_T^{(2)}$ leads to images that vary smoothly between the two corresponding endpoint images, $\mathbf{x}_0^{(1)}$ and $\mathbf{x}_0^{(2)}$.

Kwon *et al.* [14] propose *h*-space for DDMs, the set of bottleneck feature maps of the U-Net [28] across all timesteps, $\{\mathbf{h}_T, \dots, \mathbf{h}_1\}$ as the latent space. Each bottleneck feature map \mathbf{h}_t has a lower spatial dimension but more channels than the output image. They show that semantics can be edited by adding offsets $\Delta\mathbf{h}_t$ to the feature maps during the generative process. To find editing directions, they use an optimization procedure involving CLIP, where the semantics to be edited are described by text prompts. The *h*-space has the following properties: (i) a direction $\Delta\mathbf{h}_t$ typically has the same semantic effect on different samples; (ii) the magnitude of $\Delta\mathbf{h}_t$ controls the strength of the edit; (iii) *h*-space is additive in the sense that applying a linear combination of different directions where each $\Delta\mathbf{h}_t$ corresponds to a distinct attribute, results in a generated image where all attributes have been changed.

2.2. Semantic image editing in generative models

Semantic editing has been widely explored in GANs [33, 10, 6, 35, 38, 20, 24, 39, 43]. Shen *et al.* [33] used a binary classifier to annotate generated samples and trained a SVM to separate classes like pose, age, and gender. The corresponding linear directions in latent space were then defined as the normal vectors of the separating hyper-planes. Härkönen *et al.* [10] found interpretable control directions in pretrained GANs by applying principal components of latent codes to appropriate layers of the generator. Another line of work [6, 35, 38, 45] uses various factorization techniques to define meaningful directions.

Semantic image editing has also been shown in DDMs but many existing methods make adaptations to the architecture, employ text-based optimization or model fine-tuning. In DiffusionAE [21], a DDM was trained in conjunction with an image encoder. This enabled attribute manipulation on real images, including modifications of gender, age, and smile, but requires modifying the DDM architecture. Another line of work includes DiffusionCLIP [12], Imagic [11], and UniTune [41], combined CLIP-based text guidance with model fine-tuning. Unlike these methods, our approaches do not require CLIP-based text-guidance nor model fine-tuning and can be applied to existing DDMs without retraining.

3. The semantic latent space of DDMs

Diffusion models are defined in terms of a forward diffusion process that adds increasing amounts of white Gaussian noise to a clean image \mathbf{x}_0 in T steps, and a learned reverse process that gradually removes the noise. During

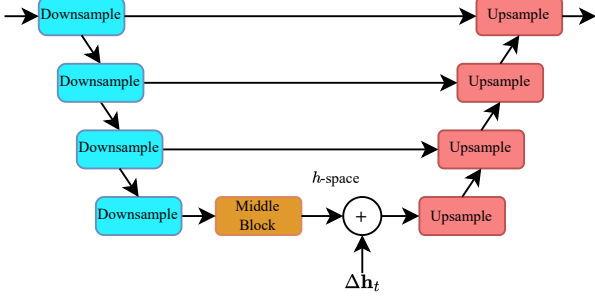


Figure 2: **Illustration of h -space.** In this paper we define the semantic latent space of DDMS as the activation after the deepest bottleneck layer of the U-Net.

the forward process each noisy image \mathbf{x}_t is generated as

$$\mathbf{x}_t = \sqrt{\alpha_t} \mathbf{x}_0 + \sqrt{1 - \alpha_t} \mathbf{n}, \quad (1)$$

where $\mathbf{n} \sim \mathcal{N}(\mathbf{0}, \mathbf{I})$ and the noise schedule is defined by $\{\alpha_t\}$. In [37], generating an image from the model is done by first sampling Gaussian noise $\mathbf{x}_T \sim \mathcal{N}(\mathbf{0}, \mathbf{I})$, which is then denoised following the approximate reverse diffusion process

$$\mathbf{x}_{t-1} = \sqrt{\alpha_{t-1}} \mathbf{P}_t(\epsilon_t^\theta(\mathbf{x}_t)) + \mathbf{D}_t(\epsilon_t^\theta(\mathbf{x}_t)) + \sigma_t \mathbf{z}_t, \quad (2)$$

where $\mathbf{z}_t \sim \mathcal{N}(\mathbf{0}, \mathbf{I})$. Here ϵ_t^θ is a neural network (usually a U-Net [28]), which is trained to predict \mathbf{n} from \mathbf{x}_t , and

$$\mathbf{P}_t(\epsilon_t^\theta(\mathbf{x}_t)) = \frac{\mathbf{x}_t - \sqrt{1 - \alpha_t} \epsilon_t^\theta(\mathbf{x}_t)}{\sqrt{\alpha_t}}, \quad (3)$$

$$\mathbf{D}_t(\epsilon_t^\theta(\mathbf{x}_t)) = \sqrt{1 - \alpha_{t-1} - \sigma_t^2} \epsilon_t^\theta(\mathbf{x}_t) \quad (4)$$

are the predicted \mathbf{x}_0 and the direction pointing to \mathbf{x}_t at timestep t , respectively. The variance σ_t is taken to be

$$\sigma_t = \eta_t \sqrt{(1 - \alpha_{t-1}) / (1 - \alpha_t)} \sqrt{1 - \alpha_t / \alpha_{t-1}}. \quad (5)$$

The special case where $\eta_t = 0$ for all t is called DDIM [37]. In this setting the noise variance is $\sigma_t = 0$, so that the sampling process is deterministic and fully reversible [8, 3] (*i.e.*, \mathbf{x}_T can be uniquely obtained from \mathbf{x}_0). The case where $\eta_t = 1$ corresponds to the stochastic DDPM scheme [8].

Following Kwon *et al.* [14], we study the semantic latent space of DDMS corresponding to the activation of the bottleneck feature maps of the U-Net (see Fig. 2). We denote the concatenation of the bottleneck activation across all timesteps by $\mathbf{h}_{T:1}$. In [14] image editing was performed via an asymmetric reverse process (Asyrp), where $\Delta \mathbf{h}_t$ is only injected into \mathbf{P}_t of (2) and not to \mathbf{D}_t . Empirically, we find that Asyrp amplifies the effect of the edits but semantic editing is also possible without using Asyrp. In this paper, we inject $\Delta \mathbf{h}_t$ into both terms of (2). This has the benefit of only

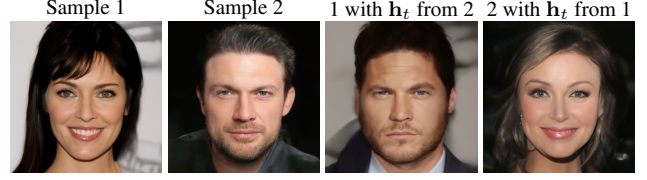


Figure 3: **Effect of swapping the bottleneck activation.** Swapping \mathbf{h}_t between two samples swaps the semantic content without affecting background and illumination.



Figure 4: **Vector arithmetic in the semantic latent space.** Adding the difference between a smiling and non-smiling person results in a smile in a new sample. Here the scale of the edit is $\gamma = 1/5$.

requiring a single forward pass of the U-Net at each step of the sampling process, as opposed to the two forward passes needed in Asyrp (one for \mathbf{P}_t with injection and one for \mathbf{D}_t without the injection). In the supplementary material (SM) Sec. A we provide a comparison of the effect of editing with and without Asyrp.

The bottleneck activation \mathbf{h}_t is determined directly from \mathbf{x}_t in each step of the generative process. It is worth noting that although most of the high-level semantic content of the generated image is determined by $\mathbf{h}_{T:1}$, it is not a complete latent representation in the sense that it does not completely specify the generated image. We illustrate this point in Fig. 3 where we swap $\mathbf{h}_{T:1}$ between two samples while keeping $\{\mathbf{x}_T, \mathbf{z}_{T:1}\}$ fixed. We observe that swapping $\mathbf{h}_{T:1}$ results in a swap of the high-level semantics, like the gender, but not the background.

A key property of h -space is that it obeys vector arithmetic properties which have previously been demonstrated for GANs by Radford *et al.* [23]. Specifically, image editing can be done in h -space as follows. Suppose we have found a direction $\mathbf{v}_{T:1}$ associated with some semantic content that we wish to apply to a sample with latent code $\mathbf{h}_{T:1}$. Then $\mathbf{h}_{T:1}^{(\text{edit})} = \mathbf{h}_{T:1} + \gamma \mathbf{v}_{T:1}$ is the latent code of the edited image, where γ controls the strength of the edit. In Fig. 4 we illustrate the vector arithmetic property of h -space.

4. Unsupervised semantic directions

4.1. Global semantic directions

Our first goal is to uncover interesting global semantic directions in an unsupervised fashion. We use the term global to refer to directions that have the same semantic

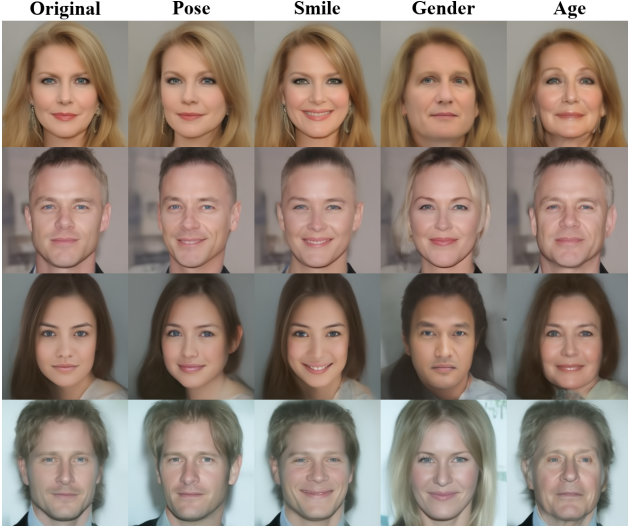


Figure 5: **Semantic directions unveiled by PCA.** PCA in h -space provides a way for discovering disentangled and semantically meaningful directions. Here we show edits corresponding to pose, smile, gender and age.

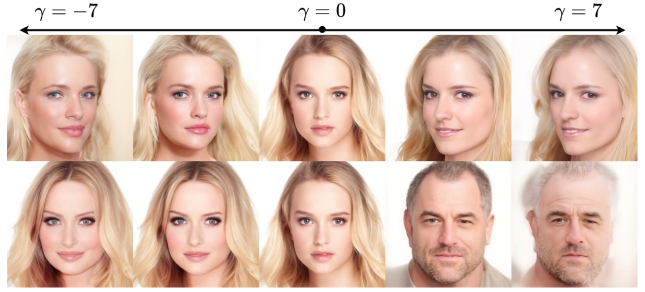
effect for all images. To this end, we explore the use of principal component analysis (PCA) in h -space. In the context of GANs [10], it was shown that the principal components of a collection of randomly sampled latent codes results in semantically interpretable editing direction. Here we demonstrate that the same is true for DDMMs if the PCA is performed in the semantic h -space.

Specifically, we consider PCA where we generate n random samples and save the bottleneck activation $\mathbf{h}_t^{(i)}$ for each sample i at all timesteps. Then, for each timestep t we vectorize $\{\mathbf{h}_t^{(i)}\}_{i=1}^n$ and calculate the principal components. We define the editing direction \mathbf{v}_j as a concatenation of the j 'th principal component from all timesteps.

To demonstrate our method, we use Diffusers [42] and a DDPM¹ trained on the CelebA [16] data set. Unless stated otherwise, all results are shown using $\eta_t = 1$ during the synthesis process. We observe that many principal directions have clear semantic interpretations, like yaw, rotation and gender. In Fig. 5 we demonstrate the effect of several of these directions, including gender (\mathbf{v}_1), pose (\mathbf{v}_2), age (\mathbf{v}_4), and smile (\mathbf{v}_{10}).

Next, we compare the effect of applying the two dominant principal components to applying random directions in Fig. 6. For a fair comparison, we set the norm of $\Delta\mathbf{h}_t$ for the random directions to match that of the principal components. While interpolating along principal directions leads to semantically interpretable edits, shifting along random direction only induces minor changes to the image at small scales and rapid degradation of the image at larger scales.

¹<https://huggingface.co/google/ddpm-ema-celebahq-256>



(a) PCA directions



(b) Random directions

Figure 6: **PCA vs. random directions.** While directions found with PCA have a clear semantic meaning, like pose and gender, interpolating along random directions results in only minor changes to the image when using the same scale. Increasing the scale results in a degradation of the image.

4.2. Discovering image-specific semantic edits

Global directions have the advantage that they are computed based on many samples and are thus applicable to any image. However, many desirable semantic edits are not applicable to all images. For example, a direction that opens or closes eyes is clearly irrelevant for a person wearing dark sunglasses. Therefore, we now focus on finding image-specific semantic directions.

To this end, we seek a set of orthogonal directions in h -space that induce the largest change in the predicted clean image $\mathbf{P}_t(\epsilon_t^\theta(\mathbf{x}_t))$ at every timestep. This is equivalent to finding the directions that change $\epsilon_t^\theta(\mathbf{x}_t)$ the most (SM Sec. E). For small perturbations, these directions are the top right-hand singular vectors of the Jacobian of ϵ_t^θ with respect to \mathbf{h}_t . Due to the skip-connections in the U-Net, the output of the network depends on both \mathbf{x}_t and \mathbf{h}_t . Yet, here we only consider the dependency on the latent variable \mathbf{h}_t .

Let \mathbf{J}_t denote the Jacobian of ϵ_t^θ w.r.t. \mathbf{h}_t , i.e.,

$$\mathbf{J}_t \triangleq \frac{\partial \epsilon_t^\theta(\mathbf{x}_t, \mathbf{h}_t)}{\partial \mathbf{h}_t}, \quad (6)$$

and denote its singular value decomposition (SVD) by

$$\mathbf{J}_t = \mathbf{U}_t \mathbf{\Sigma}_t \mathbf{V}_t^T. \quad (7)$$

Then the right singular vectors (\mathbf{V}_t 's columns) are the set of

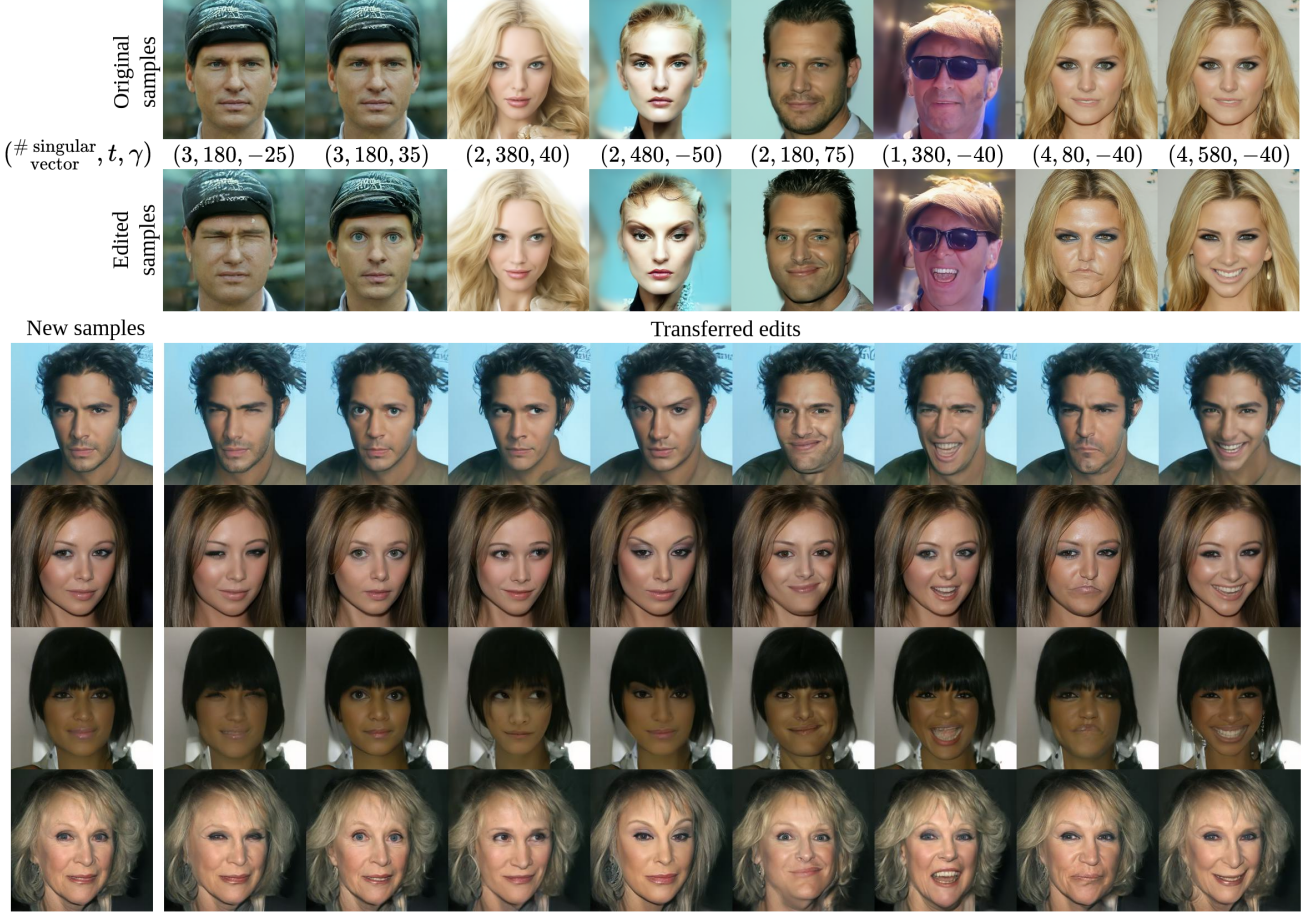


Figure 7: **Unsupervised image-specific edits.** Spectral analysis of the Jacobian of ϵ_t^θ yields directions corresponding to localized changes in the generated image, *e.g.*, eyes opening/closing and raising of the eyebrows. Although this method is image-specific, directions found for one sample can be transferred to others, where they result in semantically similar edits.

orthogonal vectors in h -space which perturb the predicted image the most. Note that for each timestep t , we have a different set of directions. In practice, we find that semantically interesting effects are obtained by applying directions found at timestep t across all timesteps. Thus, computing k directions per timestep provides us kT potential edits corresponding to the k directions found in each of the T timesteps. In SM Sec. B we illustrate the qualitative difference between directions computed at different timesteps.

In practice, calculating \mathbf{J}_t directly is very computationally expensive. Instead, we find the dominant singular vectors by power-iteration over the matrix $\mathbf{J}_t^T \mathbf{J}_t$, whose eigenvectors are precisely the right singular vectors of \mathbf{J}_t . Each iteration requires multiplication by $\mathbf{J}_t^T \mathbf{J}_t$, which can be computed without ever storing the Jacobian matrix in memory. Specifically, for any vector \mathbf{v} , the Jacobian-vector product $\mathbf{J}_t \mathbf{v}$ can be computed as the derivative

$$\mathbf{J}_t \mathbf{v} = \left. \frac{\partial}{\partial a} \epsilon_t^\theta(\mathbf{x}_t, \mathbf{h}_t + a\mathbf{v}) \right|_{a=0}. \quad (8)$$

The product $\mathbf{J}_t^T \mathbf{J}_t \mathbf{v}$ can be computed as the gradient

$$\mathbf{J}_t^T \mathbf{J}_t \mathbf{v} = \frac{\partial}{\partial \mathbf{h}_t} \langle \epsilon_t^\theta(\mathbf{x}_t, \mathbf{h}_t), \mathbf{J}_t \mathbf{v} \rangle. \quad (9)$$

The power method starts by randomly initializing a set of vectors $\{\mathbf{v}_i\}_{i=1}^k$ and iteratively computes (8) and (9) using automatic differentiation, while enforcing orthogonality among them. This is summarized in Alg. 1. Importantly, it was shown that batched power iteration with orthogonalization step, such as presented here, is guaranteed to converge to the SVD of positive semi-definite matrices [31, Ch. 5].

Our proposed method successfully identifies semantically meaningful directions that correspond to highly localized semantic changes in the image, such as closing or opening of the eyes and mouth, or raising of the eyebrows. We show a selection of such localized edits at the top of Fig. 7. While the semantic directions found by this method are image-specific and may vary depending on the sample analyzed, we find that they result in the same localized

Algorithm 1 Jacobian subspace iteration

Input: $f : \mathbb{R}^{d_{\text{in}}} \rightarrow \mathbb{R}^{d_{\text{out}}}$, $\mathbf{h} \in \mathbb{R}^{d_{\text{in}}}$ and $\mathbf{V} \in \mathbb{R}^{d_{\text{in}} \times k}$
Output: $(\mathbf{U}, \Sigma, \mathbf{V}^T) - k$ top singular values and vectors of the Jacobian $\partial f / \partial \mathbf{h}$
 $\mathbf{y} \leftarrow f(\mathbf{h})$
if \mathbf{V} is empty **then**
 $\mathbf{V} \leftarrow$ i.i.d. standard Gaussian samples
end if
 $\mathbf{Q}, \mathbf{R} \leftarrow \text{QR}(\mathbf{V})$ ▷ Reduced QR decomposition
 $\mathbf{V} \leftarrow \mathbf{Q}$ ▷ Ensures $\mathbf{V}^T \mathbf{V} = \mathbf{I}$
while stopping criteria **do**
 $\mathbf{U} \leftarrow \partial f(\mathbf{h} + a\mathbf{V}) / \partial a$ at $a = 0$ ▷ Batch forward
 $\hat{\mathbf{V}} \leftarrow \partial(\mathbf{U}^T \mathbf{y}) / \partial \mathbf{h}$
 $\mathbf{V}, \Sigma^2, \mathbf{R} \leftarrow \text{SVD}(\hat{\mathbf{V}})$ ▷ Reduced SVD
end while
 Orthonormalize \mathbf{U}

changes when applied across different images. This is illustrated at the lower part of Fig. 7 where each of the found editing directions are applied with the same magnitude γ across a selection of samples. These results suggest that our approach is effective in identifying meaningful semantic directions that generalize across different images.

Regarding implementation, in (8) we compute a derivative of high dimensional output w.r.t. a scalar. This is efficiently done by utilizing forward mode automatic differentiation. Further, (9) can be calculated in parallel for multiple vectors using the batched Jacobian-vector product, *e.g.*, in Pytorch. However, parallel calculation of a large number of vectors can be memory intensive. For such cases, we give a sequential variant of Alg.1 in SM, Sec. C.

5. Supervised discovery of semantic directions

While the methods we presented in Sec. 4 discover interpretable semantic directions in a fully unsupervised fashion, their effects must be interpreted manually. In this section, we demonstrate a simple supervised approach to obtain latent directions corresponding to well-defined labels.

Linear semantic directions from examples. The vector arithmetic property of h -space suggests an intuitive method for discovering semantically meaningful directions, by providing positive and negative examples of a desired attribute. Let $\{(\mathbf{x}_i^-, \mathbf{x}_i^+)\}_{i=1}^n$ be a collection of generated images, such that all \mathbf{x}_i^+ have a desired attribute that is absent in \mathbf{x}_i^- , *e.g.*, a smile, old age, glasses, *etc.* Let \mathbf{q}_i^- and \mathbf{q}_i^+ denote the latent representation corresponding to the images \mathbf{x}_i^- and \mathbf{x}_i^+ . Then, we can find a semantic direction \mathbf{v} as

$$\mathbf{v} = \frac{1}{n} \sum_{i=1}^n (\mathbf{q}_i^+ - \mathbf{q}_i^-). \quad (10)$$

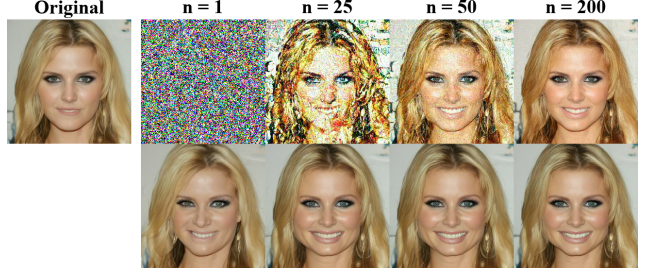


Figure 8: **Editing in h -space vs. using \mathbf{x}_T .** We qualitatively compare the effect of editing using \mathbf{x}_T (top) and $\mathbf{h}_{T:1}$ (bottom) as the latent variables using a smiling direction found by (10). While the direction in h -space converges with a few labeled examples, more than 200 are required to achieve a similar result using \mathbf{x}_T as the latent variable.

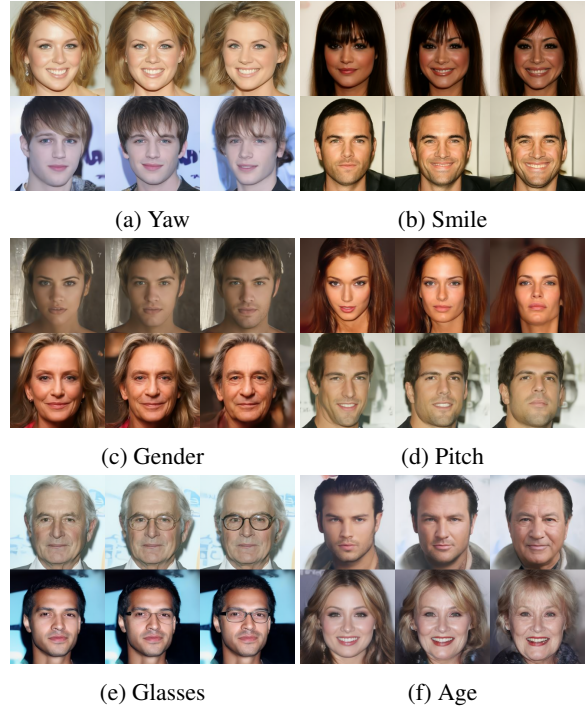


Figure 9: **Single attribute manipulation.** Using a domain-specific binary attribute classifier, we find linear directions in h -space corresponding to a variety of semantic edits.

Note that this method can be applied using either $\mathbf{h}_{T:1}$ or \mathbf{x}_T as the latent variable. Here we show that defining semantic directions using $\mathbf{h}_{T:1}$ as the latent variable requires far fewer samples than using \mathbf{x}_T . Figure 8 illustrates this for DDIM ($\eta_t = 0$) for a direction corresponding to smile where (10) is calculated using a varying number of samples.

Classifier annotation. We illustrate how to find linear semantic directions by using pretrained attribute classifiers to

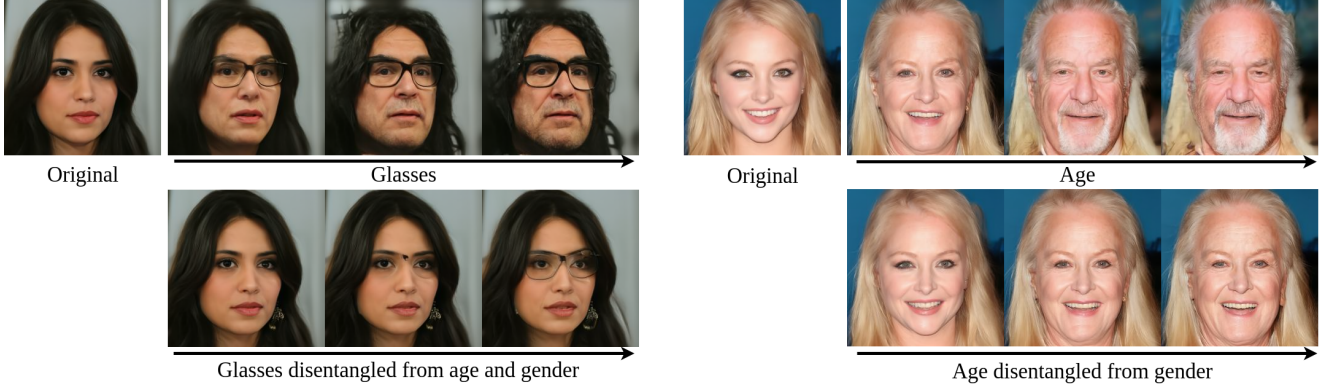


Figure 10: **Disentanglement of semantic directions.** Given a direction that is entangled with other attributes, we can create a disentangled direction by removing the projection onto undesired semantics. The top row shows the original direction, whereas the bottom row shows the disentangled direction.

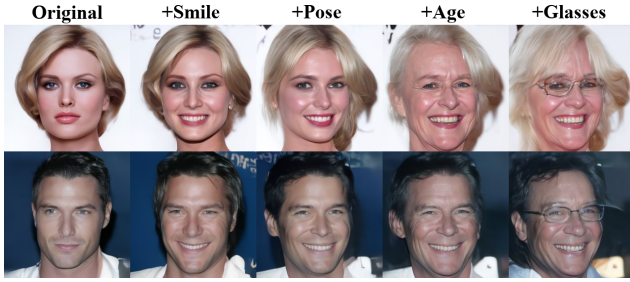


Figure 11: **Sequential manipulation.** Directions found with our method can be applied in combination with one another. Here, we sequentially accumulate four effects, starting from a single effect in the second column up to four effects in the fifth column.

annotate samples generated by the model. We use the attribute classifier from [15] to annotate samples with probabilities corresponding to the 40 classes from CelebA [16], and use Hopenet [29] to predict pose (yaw, pitch and roll). We annotate samples, sort them according to the attribute scores, select the top and bottom samples from each class and calculate a semantic direction by (10).

As shown in Fig. 9, we can successfully find semantic directions controlling a wide selection of meaningful attributes like smile, gender and glasses, as well as yaw and pitch. Furthermore, directions calculated by (10) can be applied in combination with one another. For example, adding $\Delta h_{T:1}$ for two attributes, like pose and smile, results in an image where both attributes are changed. Figure 11 illustrates sequential editing, showcasing changes in expression followed by pose, age and eyeglasses for two samples.

Disentanglement of semantic directions. Latent directions found by (10) might be semantically entangled, in the

Effect Edit	Smile	Glasses	Age	Gender	Hat
Original directions					
Smile	0.26	0.28	0.07	0.33	0.06
Glasses	0.47	0.31	0.71	0.65	0.15
Age	0.06	0.41	0.77	0.65	0.16
Gender	0.31	0.01	0.37	0.64	0.22
Hat	0.42	0.00	0.38	0.64	0.41
Disentangled directions					
Smile	0.24	0.18	0.03	0.07	0.03
Glasses	0.20	0.36	0.12	0.09	0.19
Age	0.01	0.39	0.61	0.15	0.03
Gender	0.19	0.02	0.06	0.39	0.06
Hat	0.13	0.03	0.02	0.09	0.43

Table 1: **Evaluation of disentanglement strategy.** We quantitatively evaluate the effect of disentangling semantic directions using linear projection. The rows correspond to the applied directions, while the columns correspond to the effect of the edits according to CLIP. The strongest effect in each row is highlighted.

sense that editing in the direction corresponding to some desired attribute might also induce a change in some other undesired attributes. For example, a direction for eyeglasses may also affect the age if it correlates with eyeglasses in the training data. To remedy this, we propose conditional manipulation in h -space in a way similar to what was suggested in the context of GANs by Shen *et al.* [33, 34]. Let \mathbf{v}_1 and \mathbf{v}_2 be two linear semantic directions, where the two corresponding semantic attributes are entangled. We can define a new direction $\mathbf{v}_{1\perp 2}$ which only affects the semantics associated with \mathbf{v}_1 , without changing the semantics associated with \mathbf{v}_2 . This is done simply by

removing from \mathbf{v}_1 the projection of \mathbf{v}_1 onto \mathbf{v}_2 , namely $\mathbf{v}_{1\perp 2} = \mathbf{v}_1 - \langle \mathbf{v}_1, \mathbf{v}_2 \rangle / \|\mathbf{v}_2\|^2 \mathbf{v}_2$. In case of conditioning on multiple semantics simultaneously, our aim is to remove the effects of a collection of k directions $\{\mathbf{v}_i\}_{i=1}^k$ from a primal direction \mathbf{v}_0 . This can be done by constructing the matrix $\mathbf{V} = [\mathbf{v}_1, \mathbf{v}_2, \dots, \mathbf{v}_k]$ and projecting \mathbf{v}_0 onto the orthogonal complement of the column space of \mathbf{V} by

$$\mathbf{v} = [\mathbf{I} - \mathbf{V}(\mathbf{V}^T \mathbf{V})^{-1} \mathbf{V}^T] \mathbf{v}_0. \quad (11)$$

The resulting direction will be disentangled from each of the directions $\{\mathbf{v}_i\}$, meaning that moving a sample along this new direction will result in a large change in the attribute associated with \mathbf{v}_0 while minimally affecting the attributes associated with the other directions. Figure 10 visualize the effect of interpolating in the directions of age and eyeglasses for two samples. As can be seen, these directions are entangled with gender and age, respectively. By using our method we can successfully remove the entanglement.

To validate the effectiveness of our disentanglement strategy, we performed an experiment where we edited attributes corresponding to smile, glasses, age, gender, and wearing a hat. We edited samples using both the original and the disentangled directions, while measuring the effect of each edit using CLIP [22] as a zero-shot classifier. We selected appropriate positive and negative prompts for each attribute. For smiling, glasses, and hat we used "A smiling person", "A person wearing glasses" and "A person wearing a hat" for the positive prompts respectively, and "A person" as the negative prompt. For age and gender, we used "A man" / "A woman" and "An old person" / "A young person" respectively. We edited each attribute in 1000 samples and measured the score change according to CLIP for all the attributes. Table 1 shows the results. We can see that the original directions are highly entangled with other attributes while the disentangled directions induce the largest changes in the intended attributes. This demonstrates that semantic directions can be disentangled by a simple linear projection.

Facial expressions from real data. We further show that domain-specific semantic directions can be extracted using real images as supervision. Here we use the BU3DFE data set [44]. BU3DFE contains real images of 100 subjects, each performing a neutral expression in addition to each of the prototypical facial expressions at various intensity levels. Using DDIM inversion ($\eta_t = 0$) we record $\mathbf{h}_{T:1}$ during the inversion process and use (10) to calculate directions. We use the most intense expressions for the positive examples and the neutral expressions for the negative examples. In Fig. 12 we show the effect of directions found using our method on generated samples, demonstrating that we can



Figure 12: **Facial expressions from real data.** We extract semantic directions corresponding to different facial expressions using a data set of real images. The directions are calculated via DDIM inversion and applied in the semantic h -space to synthetic images.

successfully define latent directions in h -space by using a data set of real images as supervision.

6. Discussion and conclusion

We presented several supervised and unsupervised methods for finding interpretable directions in the recently proposed semantic latent space of Denoising Diffusion Models. We showed that the principal components in latent space correspond to global and semantically meaningful editing directions like pose, gender, smile, and age. Additionally, we proposed a novel method for discovering image-specific directions that correspond to highly localized changes in generated images, such as raising the eyebrows or opening/closing of the mouth and eyes. We further showed that although these directions were found with respect to a specific image they can be transferred to different samples.

Although our unsupervised approaches are effective in discovering meaningful semantics when the DDM was trained on aligned data like human faces, we found that models trained on less structured data have less interpretable principal directions. We refer the reader to SM Sec. D for experiments on LSUN church and bedrooms.

Further, we proposed a conceptually simple supervised method utilizing the linear properties of the semantic latent space. We applied our method by finding directions corresponding to facial expressions using a data set of real images and showed that a diverse set of face semantics can be revealed using classifier annotation. Finally, we demonstrated that simple linear projection is an effective strategy for disentangling otherwise correlated semantic directions.

All of our proposed methods apply to pretrained DDMs without requiring any adaptation to the model architecture, fine-tuning, optimization, or text-based guidance.

References

- [1] Yuval Alaluf, Or Patashnik, Zongze Wu, Asif Zamir, Eli Shechtman, Dani Lischinski, and Daniel Cohen-Or. Third time's the charm? image and video editing with stylegan3. In *Computer Vision—ECCV 2022 Workshops: Tel Aviv, Israel, October 23–27, 2022, Proceedings, Part II*, pages 204–220. Springer, 2023. 2
- [2] Guillaume Couairon, Jakob Verbeek, Holger Schwenk, and Matthieu Cord. Diffedit: Diffusion-based semantic image editing with mask guidance, 2022. 1
- [3] Prafulla Dhariwal and Alexander Nichol. Diffusion models beat gans on image synthesis. In M. Ranzato, A. Beygelzimer, Y. Dauphin, P.S. Liang, and J. Wortman Vaughan, editors, *Advances in Neural Information Processing Systems*, volume 34, pages 8780–8794. Curran Associates, Inc., 2021. 1, 3
- [4] Rinon Gal, Yuval Alaluf, Yuval Atzmon, Or Patashnik, Amit H. Bermano, Gal Chechik, and Daniel Cohen-Or. An image is worth one word: Personalizing text-to-image generation using textual inversion, 2022. 1
- [5] Ian Goodfellow, Jean Pouget-Abadie, Mehdi Mirza, Bing Xu, David Warde-Farley, Sherjil Ozair, Aaron Courville, and Yoshua Bengio. Generative adversarial nets. In Z. Ghahramani, M. Welling, C. Cortes, N. Lawrence, and K. Q. Weinberger, editors, *Advances in Neural Information Processing Systems*, volume 27, page 2672–2680. Curran Associates, Inc., 2014. 1
- [6] René Haas, Stella Graßhof, and Sami Sebastian Brandt. Tensor-based emotion editing in the stylegan latent space. *arXiv:2205.06102 [cs]*, May 2022. Accepted for poster presentation at AI4CC @ CVPRW. 2
- [7] Amir Hertz, Ron Mokady, Jay Tenenbaum, Kfir Aberman, Yael Pritch, and Daniel Cohen-Or. Prompt-to-prompt image editing with cross attention control. *arXiv preprint arXiv:2208.01626*, 2022. 1
- [8] Jonathan Ho, Ajay Jain, and Pieter Abbeel. Denoising diffusion probabilistic models. In H. Larochelle, M. Ranzato, R. Hadsell, M.F. Balcan, and H. Lin, editors, *Advances in Neural Information Processing Systems*, volume 33, pages 6840–6851. Curran Associates, Inc., 2020. 3
- [9] Jonathan Ho and Tim Salimans. Classifier-free diffusion guidance. In *NeurIPS 2021 Workshop on Deep Generative Models and Downstream Applications*, 2021. 1
- [10] Erik Härkönen, Aaron Hertzmann, Jaakko Lehtinen, and Sylvain Paris. Ganspace: Discovering interpretable gan controls. In *Proc. NeurIPS*, 2020. 2, 4
- [11] Bahjat Kawar, Shiran Zada, Oran Lang, Omer Tov, Huiwen Chang, Tali Dekel, Inbar Mosseri, and Michal Irani. Imagic: Text-based real image editing with diffusion models. *arXiv preprint arXiv:2210.09276*, 2022. 1, 2
- [12] Gwanghyun Kim, Taesung Kwon, and Jong Chul Ye. Diffusionclip: Text-guided diffusion models for robust image manipulation. In *Proceedings of the IEEE/CVF Conference on Computer Vision and Pattern Recognition (CVPR)*, pages 2426–2435, June 2022. 1, 2
- [13] Gihyun Kwon and Jong Chul Ye. Diffusion-based image translation using disentangled style and content representation. *arXiv preprint arXiv:2209.15264*, 2022. 1
- [14] Mingi Kwon, Jaeseok Jeong, and Youngjung Uh. Diffusion models already have a semantic latent space. In *International Conference on Learning Representations*, 2023. 2, 3, 11
- [15] Ji Lin, Richard Zhang, Frieder Ganz, Song Han, and Jun-Yan Zhu. Anycost gans for interactive image synthesis and editing. In *IEEE Conference on Computer Vision and Pattern Recognition (CVPR)*, 2021. 7
- [16] Ziwei Liu, Ping Luo, Xiaogang Wang, and Xiaoou Tang. Deep learning face attributes in the wild. In *Proceedings of International Conference on Computer Vision (ICCV)*, December 2015. 4, 7
- [17] Chenlin Meng, Yutong He, Yang Song, Jiaming Song, Jiajun Wu, Jun-Yan Zhu, and Stefano Ermon. SDEdit: Guided image synthesis and editing with stochastic differential equations. In *International Conference on Learning Representations*, 2022. 1
- [18] Ron Mokady, Amir Hertz, Kfir Aberman, Yael Pritch, and Daniel Cohen-Or. Null-text inversion for editing real images using guided diffusion models. *arXiv preprint arXiv:2211.09794*, 2022. 1
- [19] Alex Nichol, Prafulla Dhariwal, Aditya Ramesh, Pranav Shyam, Pamela Mishkin, Bob McGrew, Ilya Sutskever, and Mark Chen. Glide: Towards photorealistic image generation and editing with text-guided diffusion models, 2021. 1
- [20] Or Patashnik, Zongze Wu, Eli Shechtman, Daniel Cohen-Or, and Dani Lischinski. Styleclip: Text-driven manipulation of stylegan imagery. In *Proceedings of the IEEE/CVF International Conference on Computer Vision (ICCV)*, pages 2085–2094, October 2021. 2
- [21] Konpat Preechakul, Nattanat Chatthee, Suttisak Wizatwongsa, and Supasorn Suwajanakorn. Diffusion autoencoders: Toward a meaningful and decodable representation. In *2022 IEEE/CVF Conference on Computer Vision and Pattern Recognition (CVPR)*, page 10609–10619, New Orleans, LA, USA, Jun 2022. IEEE. 2
- [22] Alec Radford, Jong Wook Kim, Chris Hallacy, Aditya Ramesh, Gabriel Goh, Sandhini Agarwal, Girish Sastry, Amanda Askell, Pamela Mishkin, Jack Clark, and et al. Learning transferable visual models from natural language supervision. In *Proc. ICML*, Feb 2021. arXiv: 2103.00020. 1, 8
- [23] Alec Radford, Luke Metz, and Soumith Chintala. Unsupervised representation learning with deep convolutional generative adversarial networks. In Yoshua Bengio and Yann LeCun, editors, *4th International Conference on Learning Representations, ICLR 2016, San Juan, Puerto Rico, May 2–4, 2016, Conference Track Proceedings*, 2016. 3
- [24] Yipeng Qin, Rameen Abdal, and Peter Wonka. Image2StyleGAN++: How to edit the embedded images? In *Proc. CVPR*, pages 8293–8302, Aug 2020. 2
- [25] Aditya Ramesh, Prafulla Dhariwal, Alex Nichol, Casey Chu, and Mark Chen. Hierarchical text-conditional image generation with CLIP latents. *CoRR*, abs/2204.06125, 2022. 1

- [26] Aditya Ramesh, Mikhail Pavlov, Gabriel Goh, Scott Gray, Chelsea Voss, Alec Radford, Mark Chen, and Ilya Sutskever. Zero-shot text-to-image generation, 2021. 1
- [27] Robin Rombach, Andreas Blattmann, Dominik Lorenz, Patrick Esser, and Björn Ommer. High-resolution image synthesis with latent diffusion models, 2021. 1
- [28] Olaf Ronneberger, Philipp Fischer, and Thomas Brox. U-net: Convolutional networks for biomedical image segmentation. In Nassir Navab, Joachim Hornegger, William M. Wells, and Alejandro F. Frangi, editors, *Medical Image Computing and Computer-Assisted Intervention – MICCAI 2015*, pages 234–241, Cham, 2015. Springer International Publishing. 2, 3
- [29] Nataniel Ruiz, Eunji Chong, and James M. Rehg. Fine-grained head pose estimation without keypoints. In *The IEEE Conference on Computer Vision and Pattern Recognition (CVPR) Workshops*, June 2018. 7
- [30] Nataniel Ruiz, Yuanzhen Li, Varun Jampani, Yael Pritch, Michael Rubinstein, and Kfir Aberman. Dreambooth: Fine tuning text-to-image diffusion models for subject-driven generation. *arXiv preprint arXiv:2208.12242*, 2022. 1
- [31] Yousef Saad. *Numerical methods for large eigenvalue problems: revised edition*. SIAM, 2011. 5
- [32] Chitwan Saharia, William Chan, Saurabh Saxena, Lala Li, Jay Whang, Emily Denton, Seyed Kamyar Seyed Ghasemipour, Raphael Gontijo-Lopes, Burcu Karagol Ayan, Tim Salimans, Jonathan Ho, David J. Fleet, and Mohammad Norouzi. Photorealistic text-to-image diffusion models with deep language understanding. In Alice H. Oh, Alekh Agarwal, Danielle Belgrave, and Kyunghyun Cho, editors, *Advances in Neural Information Processing Systems*, 2022. 1
- [33] Yujun Shen, Jinjin Gu, Xiaoou Tang, and Bolei Zhou. Interpreting the latent space of gans for semantic face editing. In *CVPR*, 2020. 2, 7
- [34] Yujun Shen, Ceyuan Yang, Xiaoou Tang, and Bolei Zhou. Interfacegan: Interpreting the disentangled face representation learned by gans. *TPAMI*, 2020. 7
- [35] Yujun Shen and Bolei Zhou. Closed-form factorization of latent semantics in gans. In *CVPR*, 2021. 2
- [36] Jascha Sohl-Dickstein, Eric Weiss, Niru Maheswaranathan, and Surya Ganguli. Deep unsupervised learning using nonequilibrium thermodynamics. In Francis Bach and David Blei, editors, *Proceedings of the 32nd International Conference on Machine Learning*, volume 37 of *Proceedings of Machine Learning Research*, pages 2256–2265, Lille, France, 07–09 Jul 2015. PMLR. 1
- [37] Jiaming Song, Chenlin Meng, and Stefano Ermon. Denoising diffusion implicit models. *arXiv:2010.02502*, October 2020. 2, 3
- [38] Nurit Spingarn, Ron Banner, and Tomer Michaeli. GAN Steerability without optimization. In *International Conference on Learning Representations*, 2021. 2
- [39] Ayush Tewari, Mohamed Elgharib, Gaurav Bharaj, Florian Bernard, Hans-Peter Seidel, Patrick Pérez, Michael Zöllhofer, and Christian Theobalt. StyleRig: Rigging StyleGAN for 3d control over portrait images. In *Proc. CVPR*. IEEE, June 2020. 2
- [40] Narek Tumanyan, Michal Geyer, Shai Bagon, and Tali Dekel. Plug-and-play diffusion features for text-driven image-to-image translation. *arXiv preprint arXiv:2211.12572*, 2022. 1
- [41] Dani Valevski, Matan Kalman, Yossi Matias, and Yaniv Leviathan. Unitune: Text-driven image editing by fine tuning an image generation model on a single image, 2022. 2
- [42] Patrick von Platen, Suraj Patil, Anton Lozhkov, Pedro Cuenca, Nathan Lambert, Kashif Rasul, Mishig Davaadorj, and Thomas Wolf. Diffusers: State-of-the-art diffusion models. <https://github.com/huggingface/diffusers>, 2022. 4
- [43] Zongze Wu, Dani Lischinski, and Eli Shechtman. Stylespace analysis: Disentangled controls for StyleGAN image generation. In *Proc. CVPR*, Dec 2020. 2
- [44] Lijun Yin, Xiaozhou Wei, Yi Sun, Jun Wang, and M.J. Rosato. A 3d facial expression database for facial behavior research. In *7th Intern. Conf. on Automatic Face and Gesture Recognition (FGR06)*, pages 211–216, 2006. 8
- [45] Jiapeng Zhu, Ruili Feng, Yujun Shen, Deli Zhao, Zhengjun Zha, Jingren Zhou, and Qifeng Chen. Low-rank subspaces in GANs. In *Advances in Neural Information Processing Systems (NeurIPS)*, 2021. 2

Supplemental Materials

A. The effect of Asyrp

In the main text we stated that using Asyrp [14] acts to amplify the effect edits in h -space. However, Asyrp is computationally costly since it requires two forward passes of the U-Net at each denoising step. Hence, Asyrp is not used for any of the results shown in the main paper. In Figs. 13 and 14 we qualitatively compare edits with and without using Asyrp. We observe that simply adjusting the scale of the applied direction results in very similar edits.

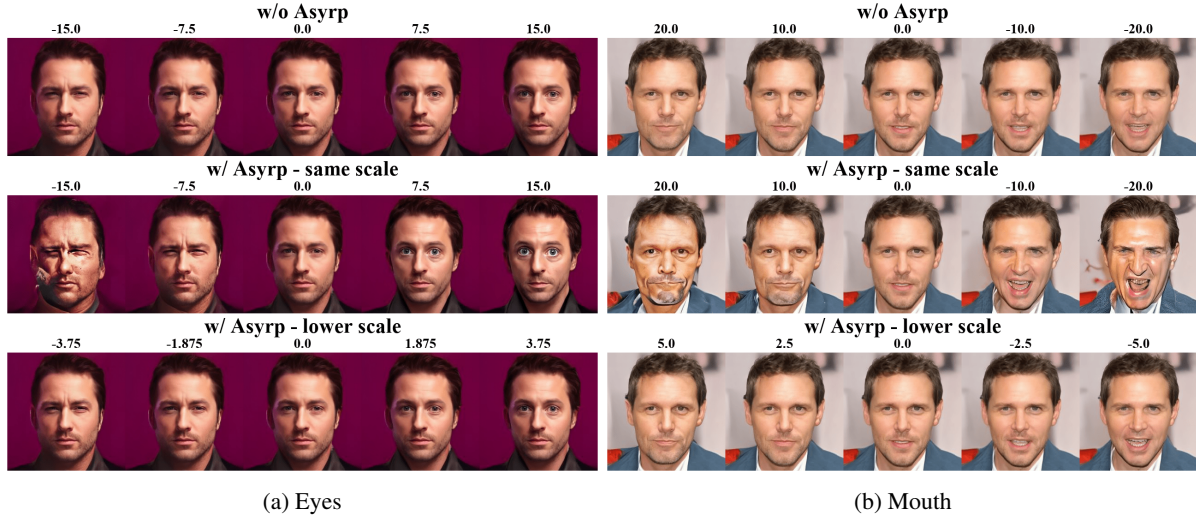


Figure 13: **The Effect of Asyrp.** Results are shown for directions found with Alg. 1.

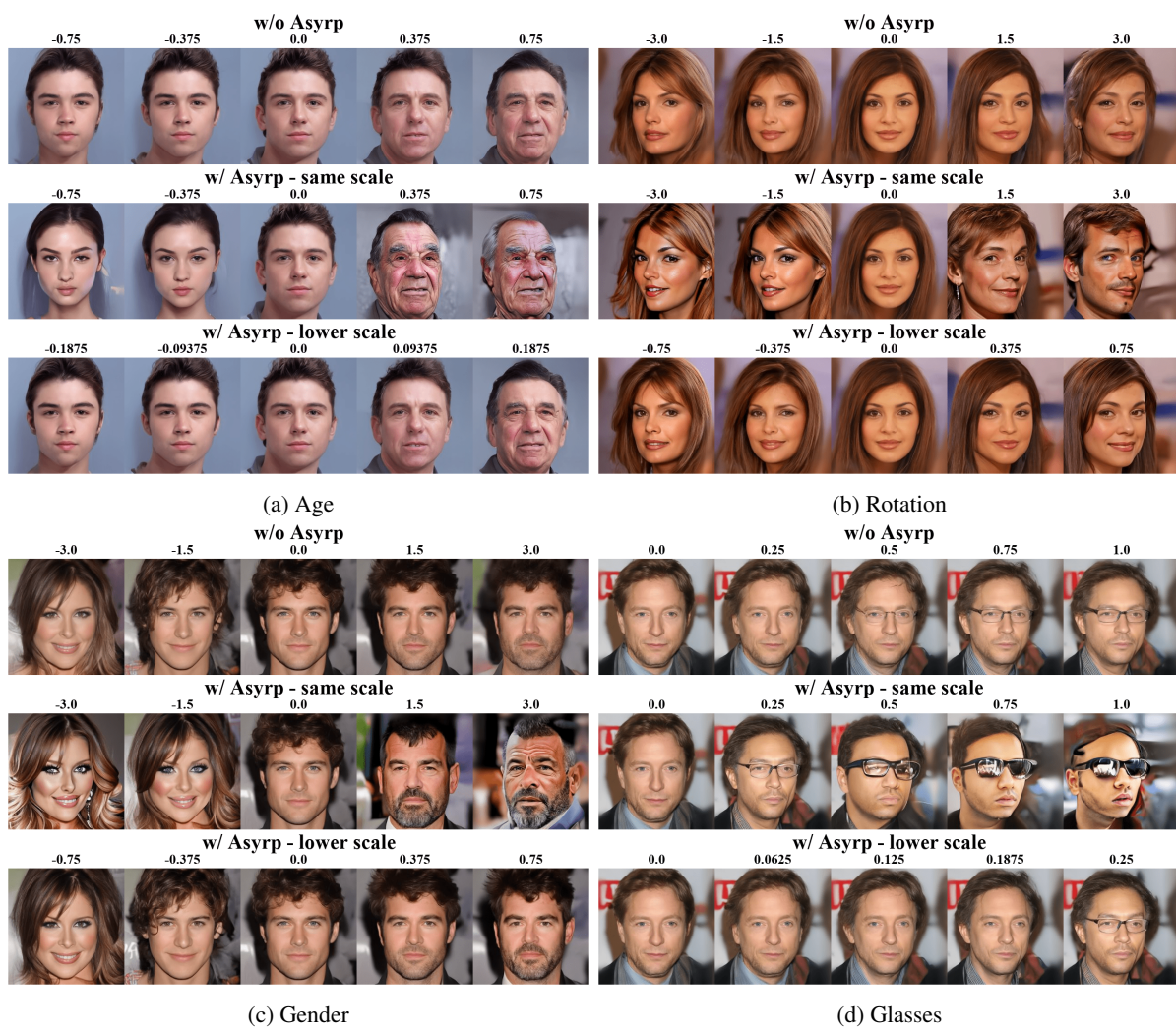


Figure 14: **The effect of Asyrp.** Results are shown for directions found using classifier annotation.

B. Image-specific directions at different timesteps

Our proposed image-specific unsupervised method in Alg. 1 finds different directions for each timestep. In Figures 15, 16, 17 and 18 we show the effect of the three dominant directions (the three top singular vectors of the Jacobian) at different timesteps along the reverse diffusion process.



Figure 15: Directions found by Alg. 1.



Figure 16: Directions found by Alg. 1.



Figure 17: Directions found by Alg. 1.



Figure 18: Directions found by Alg. 1.

C. Sequential algorithm for Jacobian subspace iteration

As mentioned in the main text, Alg. 1 can be memory intensive when calculating a large number of singular vectors in parallel. In cases where limited memory is available, we provide an alternative sequential version of our method in Alg. 2. Here we calculate the singular values and vectors in mini-batches of size b . The value of b should be set according to the parallel computation capacity. For example, in the special case of $b = 1$, the algorithm computes the vectors one by one and will use small memory. Note that lowering the mini-batch size b comes at the expense of longer running time.

Algorithm 2 Sequential Jacobian subspace iteration

Input: function to differentiate $\mathbf{f} : \mathbb{R}^{d_{\text{in}}} \rightarrow \mathbb{R}^{d_{\text{out}}}$, point at which to differentiate $\mathbf{h} \in \mathbb{R}^{d_{\text{in}}}$, initial guess $\Theta \in \mathbb{R}^{d_{\text{in}} \times k}$ [optional], mini-batch size $b < k$

Output: $(\mathbf{U}, \Sigma, \mathbf{V}^T) - k$ top singular values and vectors of the Jacobian $\partial \mathbf{f} / \partial \mathbf{h}$

Initialization: $\mathbf{y} \leftarrow \mathbf{f}(\mathbf{h})$, $i_{\text{start}} \leftarrow 1$, $i_{\text{end}} \leftarrow b$, $\mathbf{V} \leftarrow []$, $\Sigma \leftarrow []$, $\mathbf{U} \leftarrow []$

while $i_{\text{start}} \leq k$ **do**

if Θ is empty **then**

$\Phi \leftarrow$ i.i.d. standard Gaussian samples in $\mathbb{R}^{d_{\text{in}} \times (i_{\text{end}} - i_{\text{start}} + 1)}$

else

$\Phi \leftarrow$ columns i_{start} to i_{end} of Θ

end if

$\mathbf{Q}, \mathbf{R} \leftarrow \text{QR}(\Phi)$ ▷ Reduced QR decomposition

$\Phi \leftarrow \mathbf{Q}$ ▷ Ensures $\Phi^T \Phi = \mathbf{I}$

while stopping criterion **do**

if \mathbf{V} is not empty **then**

$\Phi \leftarrow [\mathbf{I} - \mathbf{V}(\mathbf{V}^T \mathbf{V})^{-1} \mathbf{V}^T] \Phi$

$\Phi, \mathbf{R} \leftarrow \text{QR}(\Phi)$ ▷ Reduced QR decomposition

end if

$\Psi \leftarrow \partial \mathbf{f}(\mathbf{h} + a\Phi) / \partial a$ at $a = 0$ ▷ Batch forward

$\hat{\Phi} \leftarrow \partial(\Psi^T \mathbf{y}) / \partial \mathbf{h}$

$\Phi, \mathbf{S}, \mathbf{R} \leftarrow \text{SVD}(\hat{\Phi})$ ▷ Reduced SVD

end while

$\mathbf{V} \leftarrow [\mathbf{V}; \Phi]$

$\Sigma \leftarrow \begin{bmatrix} \Sigma & \mathbf{0} \\ \mathbf{0} & \mathbf{S}^{1/2} \end{bmatrix}$

$\mathbf{U} \leftarrow [\mathbf{U}; \Psi]$

$i_{\text{start}} \leftarrow i_{\text{start}} + b$

$i_{\text{end}} \leftarrow \min\{i_{\text{end}} + b, k\}$

end while

Orthonormalize \mathbf{U}

D. Unsupervised methods on other domains

In addition to the model² trained on CelebA, which is used throughout the main paper, we also conducted experiments with models trained on churches³ and bedrooms⁴. Although the unsupervised directions found with both PCA and Alg. 1 on these models lead to various changes to the images, these directions are less interpretable than those obtained for faces in the main paper. We showcase the first 5 PCA directions on the models trained on churches and bedrooms in Figures 19 and 20 and directions found using Alg. 1 in Figures 22 and 21.

²<https://huggingface.co/google/ddpm-ema-celebahq-256>

³<https://huggingface.co/google/ddpm-ema-church-256>

⁴<https://huggingface.co/google/ddpm-ema-bedroom-256>

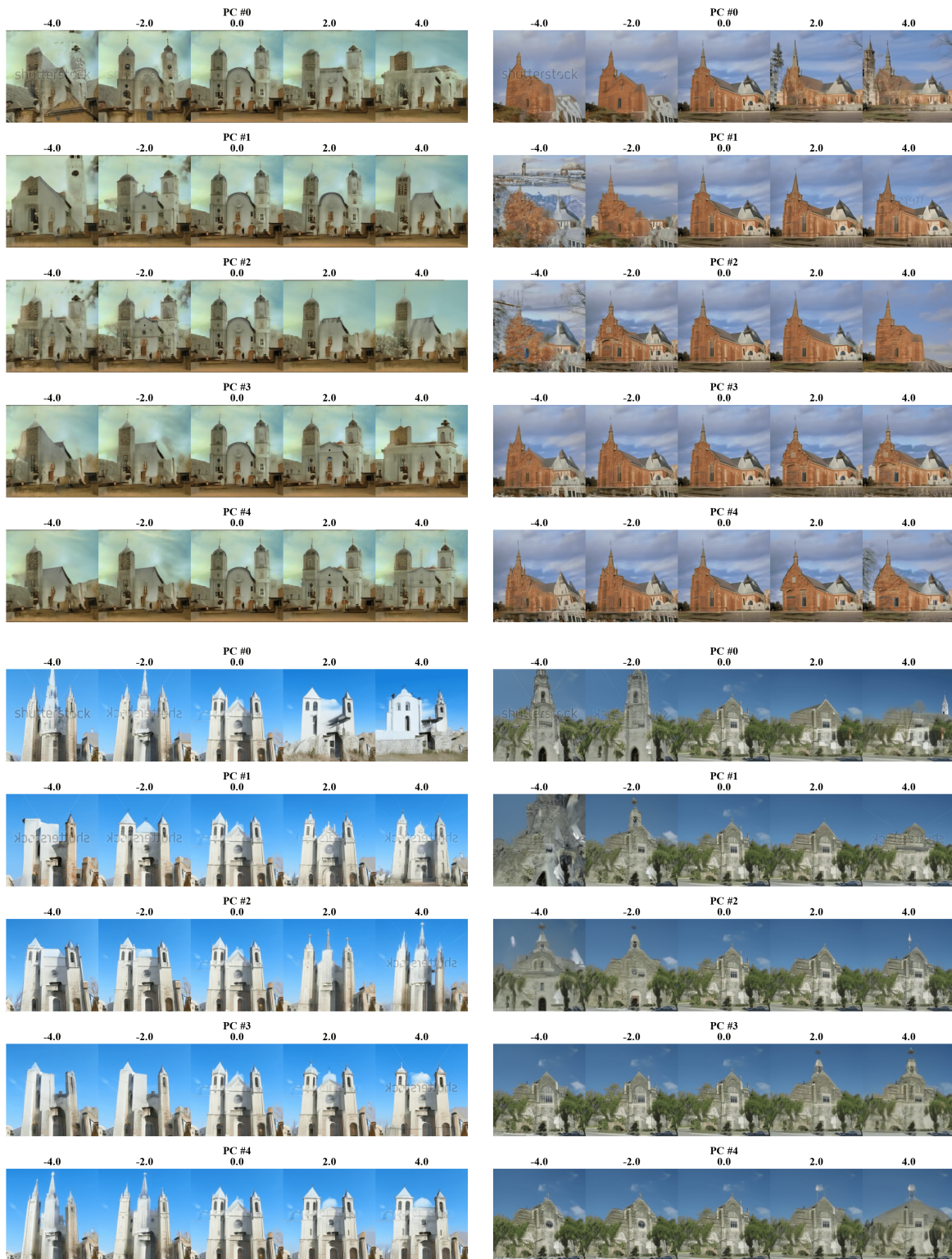


Figure 19: **PCA directions.** For a DDM trained on churches.

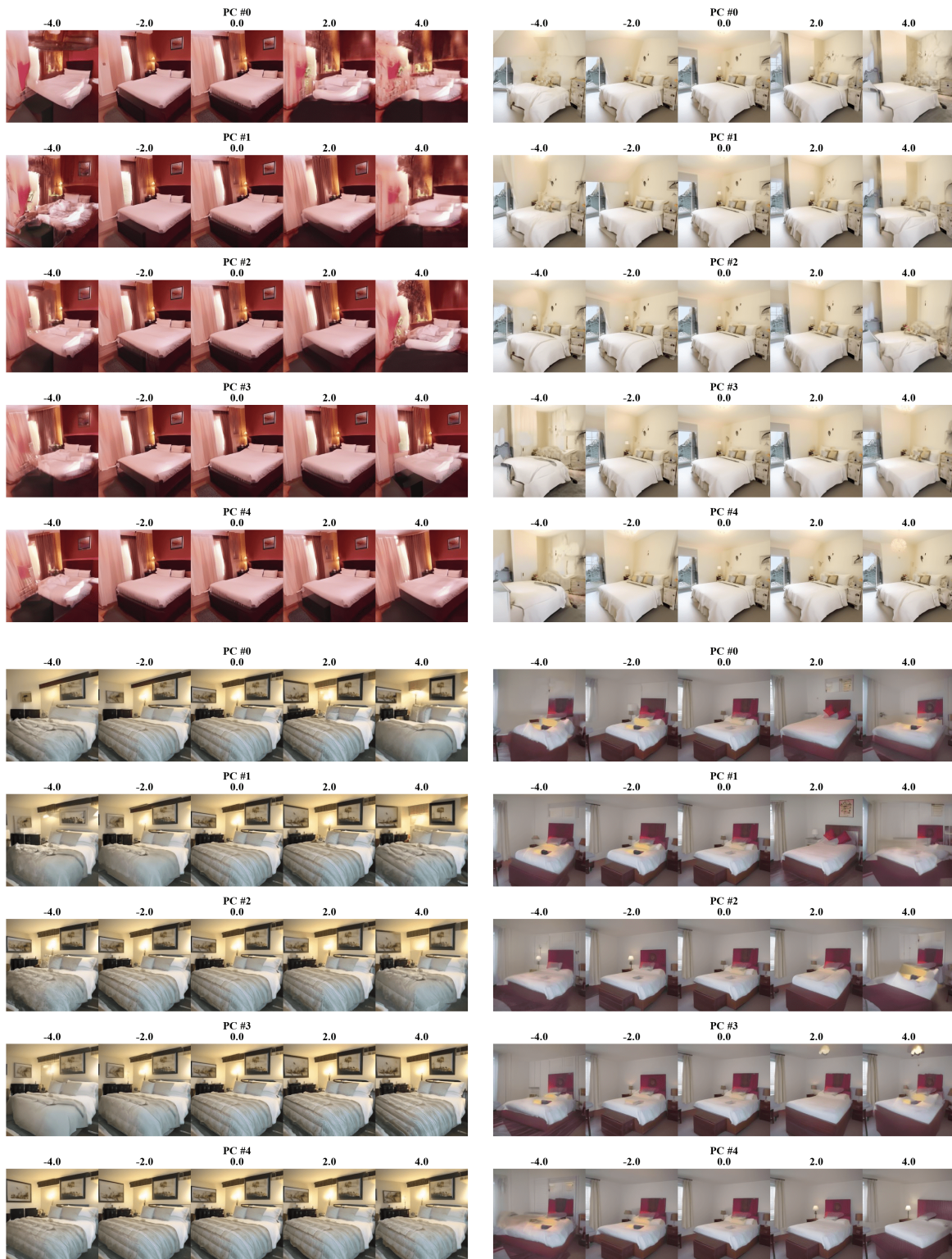


Figure 20: **PCA directions.** For a DDM trained on bedrooms.



Figure 21: **Directions** found with Alg. 1. For a DDM trained on bedrooms.



Figure 22: Directions found with Alg. 1. For a DDM trained on churches.

E. A Note on image-specific directions

In the main paper, we state that the right singular vectors of the Jacobian of ϵ_t^θ with respect to h -space, denoted as \mathbf{J}_t , are the set of orthogonal vectors in h -space which perturb the noise prediction ϵ_t^θ the most. An equivalent statement is that those right singular vectors perturb the predicted image $\mathbf{P}_t(\mathbf{x}_t, \mathbf{h}_t)$ at timestep t the most. Specifically, since

$$\mathbf{P}_t(\mathbf{x}_t, \mathbf{h}_t) = \frac{\mathbf{x}_t - \sqrt{1 - \alpha_t}}{\sqrt{\alpha_t}} \epsilon_t^\theta(\mathbf{x}_t, \mathbf{h}_t) \quad (12)$$

we have that

$$\frac{\partial}{\partial \mathbf{h}_t} \mathbf{P}_t(\mathbf{x}_t, \mathbf{h}_t) = -\frac{\sqrt{1 - \alpha_t}}{\sqrt{\alpha_t}} \frac{\partial}{\partial \mathbf{h}_t} \epsilon_t^\theta(\mathbf{x}_t, \mathbf{h}_t) = -\frac{\sqrt{1 - \alpha_t}}{\sqrt{\alpha_t}} \mathbf{J}_t. \quad (13)$$

Thus, the eigenvectors of $(\partial \mathbf{P}_t / \partial \mathbf{h}_t)^\top (\partial \mathbf{P}_t / \partial \mathbf{h}_t)$ and $\mathbf{J}_t^\top \mathbf{J}_t$ are the same with the same ordering.